Eur Biophys J (1998) 27: 391–402

ARTICLE

Laurence Salomé · Jean-Luc Cazeils · André Lopez
Jean-François Tocanne

Characterization of membrane domains by frap experiments at variable observation areas

Received: 4 September 1997 / Revised version: 19 January 1998 / Accepted: 19 January 1998

Abstract In this paper we show that FRAP experiments at variable beam radii provide an experimental approach for investigating membrane organization and dynamics, with great potential for identifying micrometer-sized domains and determining their size and the diffusion coefficient of the lipid and protein molecules they contain. Monte Carlo simulations of FRAP experiments at variable beam radii R on models of compartmentalized membranes have allowed us to establish the relationships (i) between the mobile fraction M of a diffusing particle and the size r of the domains, and (ii) between the apparent diffusion coefficient D_{app} and the real diffusion coefficient D_0 of this particle inside the domains. Furthermore, in its present stage of development, this approach allows us to specify whether these domains are strictly closed or not. This approach was first validated on an experimental model of a strictly compartmentalized membrane consisting of a monolayer of apposed spherical phospholipid bilayers supported by silica beads of known radius (0.83 μm). To prevent fusion between the spherical bilayers 5 mol% of a polymer-grafted phospholipid was added to the lipids. Analysis of the M versus R data yielded a radius r of 0.92±0.09 μm for the spherical bilayers, close to that of the supporting silica beads. When applied to the experimental data available for lipids and proteins in the plasma membrane of living cells, this approach suggests the existence of domains within these membranes with a radius of about 0.4–0.7 μm for the lipids and 0.25 μm for the proteins. These domains are not strictly closed and they are believed to be delineated by fluctuating barriers which are more or less permeable to lipid and protein molecules.

Key words Lipid and protein lateral diffusion · Mobile fraction · Membrane lateral organization · Spherical and planar supported bilayer · Polymer-grafted phospholipid · Numerical simulations

Based on a presentation at the EBSA European Biophysics Congress, Orléans, France, July 1997.

L. Salomé · J.-L. Cazeils · A. Lopez (✉) · J.-F. Tocanne
Institut de Pharmacologie et Biologie Structurale,
118 Route de Narbonne, F-31062 Toulouse Cedex, France
e-mail: lopez@ipbs.fr

Introduction

Biological membranes are far from being homogeneous mixtures of their lipid and protein components (Jacobson et al. 1995). It is now well established that small scale heterogeneities arise in the lateral distribution of lipids (De Bony et al. 1989; Tocanne 1992; Welby et al. 1996; Mouritsen and Jorgensen 1997) and proteins at sites of enzymatic pathways (Sweet and Schroeder 1988) and that larger scale lateral heterogeneities corresponding to the existence of micrometer-sized domains also have to be considered (Welti and Glaser 1994; Tocanne et al. 1994 a).

Micrometer-sized domains have been directly revealed during the study of the lateral motion of transferrin and α_2-macroglobulin receptors in the plasma membrane of cultured normal rat kidney fibroblastic cells using a single particle tracking (SPT) technique coupled with laser tweezers (Sako and Kusumi 1994, 1995). This approach showed the presence of "fences", probably proteic in nature, delineating domains in which the receptor molecules were free to diffuse laterally, and with the possibility of slow intercompartmental movements. These observations led to the proposal of a new model of a membrane of the 'confined' type (Sako and Kusumi 1995; Kusumi and Sako 1996). If the notion of closed domains has been borne out for certain membrane proteins (Sako and Kusumi 1994, 1995; Simson et al. 1995), the same kind of lateral compartmentalization has not yet been directly detected for lipids, and the origin of the heterogeneities observed in the lateral distribution of these molecules remains to be identified.

The technique of Fluorescence Recovery After Photobleaching (FRAP) has long been recognized as a powerful tool for investigating the long range lateral motion of lip-

ids and proteins in membranes (Axelrod et al. 1976; Vaz et al. 1982; Edidin 1993; Tocanne et al. 1994 b). Two parameters are obtained: D, the lateral diffusion coefficient and M, the mobile fraction of the diffusing species. When the radius R of the illuminated area is small compared to the radius r_d of the diffusion area ($r_d/R > 5$, condition of an infinite reservoir) and for freely diffusing species, M must be equal to 1 (Lopez et al. 1988). In fact, most of the FRAP data reported so far for lipids and proteins in biological membranes (with the condition of an infinite reservoir being satisfied) shows the existence of an immobile fraction which can be considered as a strong indication that the membrane is structured laterally (Tocanne et al. 1994 b). We recently published numerical simulations of FRAP experiments in which a membrane lipid leaflet was modeled using a triangular lattice of diffusing tracers obstructed with immobile obstacles of various sizes and surface concentrations (Schram et al. 1994). These simulations were designed to study the influence of proteins on the lateral diffusion of lipids. Interestingly, and for point obstacle surface concentrations above the percolation threshold, it was shown that an increase in R was accompanied by an increase in D and a decrease in M, associated with the existence of closed domains whose average size and diffusion parameters could be determined (Schram et al. 1994). In the plasma membrane of human fibroblasts (Yechiel and Edidin 1987), and hepatoma cells (Edidin and Stroynowski 1991), the D and M values measured for proteins and lipids with increasing R had been reported to increase and decrease respectively, thus suggesting the existence of closed diffusion domains in these membranes (Schram et al. 1994). However, for proteins it has recently been shown that the detection of an immobile fraction may reflect not only a microcompartmentation of the diffusion area but possibly an anomalous translational diffusion of the molecules (Feder et al. 1996). Because the FRAP technique enables the long range translational motion of both proteins and lipids to be studied, we decided to further investigate the potential of FRAP experiments at variable illumination beam radius R in detecting membrane domains and in characterizing their size and diffusion properties. To this end, Monte Carlo simulations of FRAP experiments at variable beam radius R were performed on membranes represented by a 150×150 site triangular lattice obstructed by fences delineating hexagonal closed or slightly open diffusion areas of different sizes. From the dependence of M and D on R, we show that it is possible to demonstrate the presence of strictly closed or slightly open domains in a membrane and to evaluate their average size and the true diffusion coefficient of the particles which freely diffuse within these domains. This approach was validated using an experimental model of compartmentalized membrane consisting of a monolayer of apposed spherical phospholipid bilayers supported by silica beads of known radius, and then applied to the above mentioned FRAP data obtained for proteins and lipids in the plasma membrane of human fibroblasts (Yechiel and Edidin 1987), and hepatoma cells (Edidin and Stroynowski 1991).

Materials and methods

Materials

Egg yolk phosphatidylcholine (eggPC) and N-(7-nitrobenz-2-oxa-1,3-diazol-4-yl)-phosphatidylethanolamine from eggPC (NBD-egg-PE) in powder form, and polyethyleneglycol (Mw = 5000 Da) covalently linked to a phosphatidylethanolamine (1-palmitoyl-2-oleoyl-*sn*-glycero-3-phosphoethanolamine-N-[poly(ethylene glycol)] (PEG5000-eggPE)) in chloroformic solution were purchased from Avanti Polar Lipids Inc. (Alabaster, AL). The silica beads were monodisperse in size and spherical with a radius of 0.83 μm, they were kindly supplied by Dr. C. Guénoun-Amiel (Laboratoire de Physicochimie des Biopolymères – CNRS, Thiais). Ultra-pure water was used (Milli-Q Plus quality from Millipore). Solvents and salts were of analytical grade.

Preparation of small unilamellar vesicles

They were prepared as described in Bayerl et al. (1990). Chloroform solutions of given lipids were mixed to achieve the desired molar ratio. (In all cases, the NBD-eggPE to host phospholipid molar ratio was kept constant and equal to 2%). The solvent was evaporated at 40 °C under a stream of nitrogen and then *in vacuum* for 30 min. The dry lipids were dispersed in 1 ml of a 100 mM NaCl solution by vigorous vortexing and the dispersion was sonicated for 15 min using a Branson tip sonifier (30 W output power, pulsed mode with 50% duty cycle, Branson Sonic Power Co., Danbury, CT). During sonication the sample was immersed in a water bath in order to keep its temperature below 50 °C. The vesicle suspensions so obtained were used immediately for the preparation of spherical supported lipid bilayers.

Preparation of spherical supported lipid bilayers

Firstly, single phospholipid bilayers were adsorbed on spherical silica beads using the procedure described by Bayerl et al. (1990) with slight modifications. Silica beads (2 mg) were washed twice in methanol (1 ml), then four times in water (0.5 ml) and finally once in 100 mM NaCl (0.5 ml). At each step, the beads were dispersed in the washing solution by vigorous vortexing. If aggregates remained in the dispersion, they were eliminated by a sonication step in a sonication bath. After each washing step, the beads were centrifuged in a desktop centrifuge (1000 rpm, 3 min) and the supernatant was discarded. After the last washing step, 100 mM NaCl (100 μl) was added to the beads. Then, the SUV (1 ml suspension at a concentration of 0.3 mg/ml) were added and the mixture was placed in a sonication bath for 5 min before being vigorously vortexed for 2 min. The SUV adsorbed at the surface of the beads and fused to form a continuous single

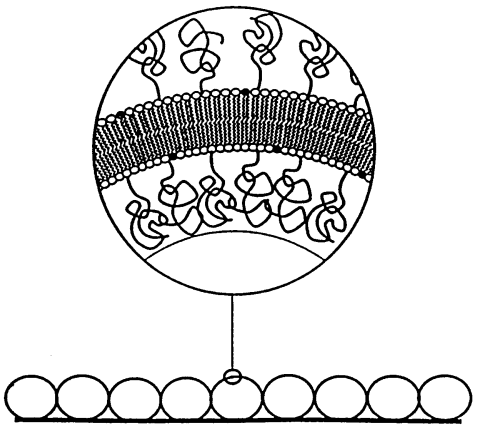

Fig. 1 Schematic representation of a monolayer of apposed spherical silica-bead-supported lipid bilayers. The inset shows the "hairy" lipid bilayer with the polymer-grafted and head-labeled phospholipids, adsorbed at the bead surface

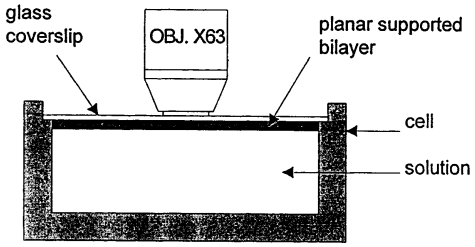

Fig. 2 Schematic diagram of the sample cell used for FRAP experiments on supported planar lipid bilayers

phospholipid bilayer on each, thus leading to spherical supported lipid bilayers (SSB) (Fig. 1). The SSB were rinsed three times in 100 mM NaCl (1 ml) by centrifugation. Direct observation in a fluorescence microscope showed that under these conditions the beads were uniformly labeled and that the excess SUV, which did not participate in the formation of spherical supported bilayers, were eliminated.

Secondly, a monolayer of SSB was prepared by depositing 1 µl of the SSB suspension (without aggregates) between a slide and a coverslip (18×18 mm^2) and pressing them between two magnets in order to force the suspension to spread over the whole space available with a reproducible pressure. Before observation in the microscope, the preparations were sealed with fingernail polish. The silica beads had a mean diameter of 1.66 µm. In the microscope, a distance of ~3 µm was measured between the slide and the coverslip, less than twice the diameter of a SSB, thus indicating the absence of multilayers of SSB.

Preparation of planar supported lipid bilayers

Planar supported lipid bilayers were formed on cleaned coverslips mounted on a small tank adapted to the microscope stage (see Fig. 2 for a schematic representation of the sample cell). The cleaning procedure of the coverslips was of great importance with respect to the formation of the bilayer. Coverslips were first sonicated in methanol for 5 min, dried in an oven for 15 min at 110 °C, immersed in sulfochromic acid for 1 h and then rinsed extensively with water (15 times in a large volume of water). These clean coverslips were kept in water (replaced daily) for no more than 5 days. Just before use, a coverslip was taken out of water and placed on the top of the sample cell. The cell was filled with the SUV suspension (diluted to a concentration of 0.2 mg/ml), up to contact of the water phase with the coverslip. The whole set up was then immersed in a sonication bath for 5 min. SUV adsorbed at the surface of the coverslip and fused to form a single planar supported lipid bilayer within a few minutes (Kalb et al. 1992). After 30 min, the cell was washed for 1 h with a 100 mM NaCl solution using a peristaltic pump, at a flow rate of 65 ml/h. Finally, the cell was further kept at rest for 1 h before starting FRAP experiments.

FRAP experiments

FRAP experiments were carried out under conditions of constant incident light intensity and uniform disk illumination, in an epifluorescence microscope (Ortholux II, Leitz) equipped with a conventional mercury arc lamp and a correct combination of a dichroic-mirror and optical filters for the NBD fluorophore. Both the apparatus and the experimental procedure have been described elsewhere (Lopez et al. 1988). A ×63/1.3 oil-immersion objective and a set of diaphragms allowing the radius R of the observation area to be varied between 1.05 µm and 8.75 µm were used. Experiments were performed at room temperature (~20 °C), with a bleaching time not exceeding 10% of the characteristic diffusion time. For each R value tested, 30 recoveries were recorded at different locations in the sample under study.

Numerical simulation of FRAP experiments

The computer generation of simulated FRAP experiments has already been described in detail (Schram et al. 1994). In this report, we will just consider the features which are important with respect to the specific case we studied. The membrane is represented by a 150×150 site triangular lattice. Each site can be empty or bear an immobile obstacle or a tracer. Lateral diffusion of tracers is followed by sequential reading of all the matrix sites. One reading of the matrix defines a time-step, the time unit of the system. When a tracer is found on a site, a jump direction, from this site to one of the six closest neighbors, is chosen at random. Because tracers are considered as being independent, two tracers or more are allowed to occupy the same

site. Therefore, if the site chosen for the jump is free or occupied by a tracer, the jump can occur. If the site under consideration bears more than one tracer, the process is repeated until all tracers have been examined. If the site chosen is occupied by an obstacle, then the jump is not allowed to occur and the tracer stays in its initial site until the next time-step. Owing to the finite size of the matrix, periodic boundary conditions were used for tracers. In order to generate a recovery curve, point obstacles were introduced and arranged in the matrix in a honeycomb network defining juxtaposed strictly closed or slightly open hexagonal domains of side h (in lattice spacing units, l.s.). In the following, the size of the hexagons will be referred to as the radius r of the circular disk of equivalent area (r = 0.909 h). The position of the hexagon network in the matrix was chosen at random and changed from one simulation to another. Then, 4000 point tracers were distributed randomly on the lattice. In each closed domain, tracers were free to diffuse laterally. For the simulation of FRAP experiments, a circular area of observation, of radius R, was introduced at the center of the matrix. The initial fluorescence intensity Io was determined by computing the average number of tracers present inside the observation area over 100 time-steps. To simulate the bleaching step, all the tracers present in the observation area were suppressed. For the recovery step, the fluorescence intensity I(t) was evaluated by calculating at each time-step the number of tracers which had returned to the observation area, and that over a number of time-steps sufficient for a complete re-equilibration of tracers to be reached. Thus, from 400 to 1800 time-steps were required when increasing r from 4.5 l.s. to 36.4 l.s. For the various r and R values tested, it was important to achieve good sampling of the system. This condition was satisfied by testing all possible configurations of the hexagon network with respect to the observation area. Thus, 250 to 750 FRAP experiments were accumulated and averaged to build the corresponding recovery curve I(t)/Io.

Fig. 3 A–C Simulated FRAP experiments with closed domains. Snapshots are shown illustrating three steps of the simulation: **A** before bleaching, **B** immediately after bleaching, **C** during the recovery process. The tracers are indicated by the *yellow dots*. The radius observed (*red circle*) was R = 25 l.s. (*lattice spacing*) and the size of hexagons (delimited by the *blue site-obstacles*) was r = 9.09 l.s. (See text for details)

We checked that the D and M solution values remained unchanged upon further accumulation of FRAP experiments. In these FRAP simulations D is given in units $u = (l.s.)^2$/time step.

Analysis of FRAP data

With the exception of the monolayers of spherical supported bilayers which will be discussed later, the diffusion coefficient D and the mobile fraction M were obtained by fitting classical equations of diffusion to the experimental and simulated recovery curves, as already described (Lopez et al. 1988). A minimization algorithm coupled to statistical analysis of the data was used which, from a set of accumulated recovery curves, provides the solution value for D and M and their maximum (D_{max}, M_{max}) and minimum (D_{min}, M_{min}) values for a certain degree of confidence (Lopez et al. 1988). In the present work, D and M are given at a 95% confidence level.

The determination of theoretical mobile fractions through image analysis of simulated and real FRAP experiments was carried out with the Adobe Photoshop software version 2.5.1 of Adobe Systems Incorporated (USA).

Results

Numerical FRAP experiments on simulated partitioned membranes

Figure 3 shows snapshots illustrating three steps of the simulated FRAP experiments: before bleaching, just after bleaching and during the recovery process. The diffusion of the tracers was restricted to the inside of the hexagonal domains within which they had fallen during the initial random distribution of the tracers. After the bleaching step, only the remaining tracers belonging to those domains which straddle the observation area could contribute to the "fluorescence" recovery inside the bleached area. During the diffusion process these tracers redistributed themselves inside their respective domain, leading to the presence of a certain fraction of them inside the observation area after equilibrium was reached.

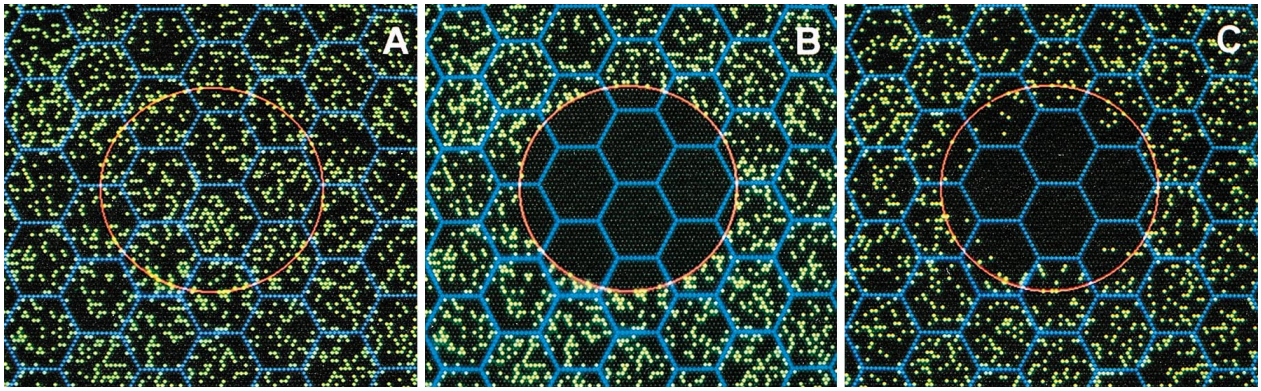

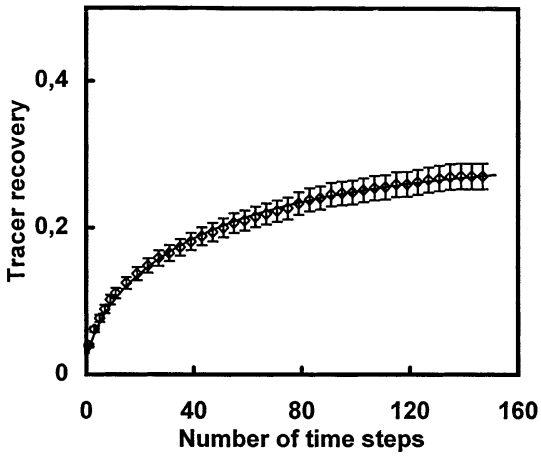

Fig. 4 Simulated FRAP experiments with closed domains. *Open squares:* recovery curve averaged from one hundred simulations performed with a beam radius R = 16 l.s. and a hexagon size r = 9.09 l.s. *Solid line:* best fit of the diffusion equation to the data yielding a M value of 0.32±0.01

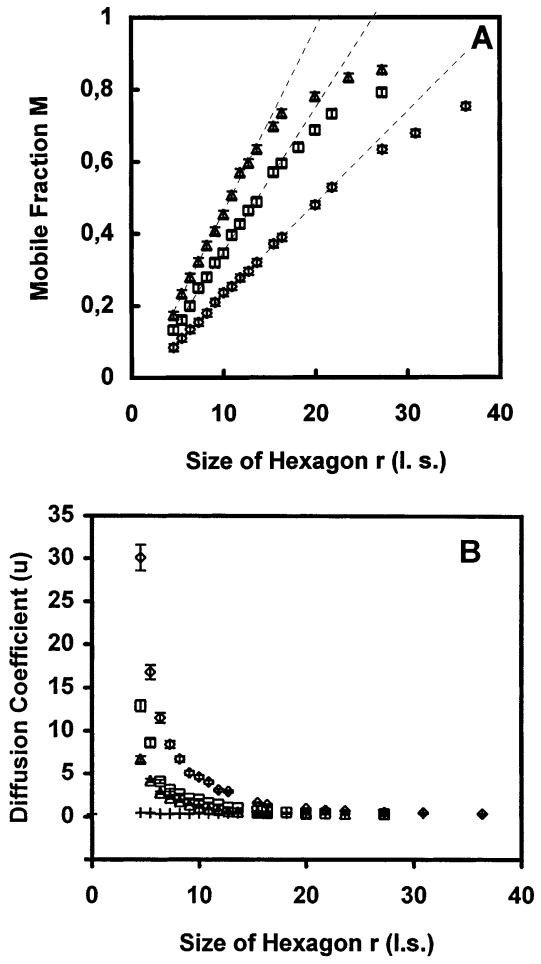

Fig. 5 A, B Simulated FRAP experiments with closed domains. Influence of the hexagon size r on **A**, the mobile fraction M and **B**, the apparent diffusion coefficient D_{app} for various values of the beam radius R. R was 12 l.s. (△), 16 l.s. (□) and 25 l.s. (◇). Also shown are the D_0 values calculated from D_{app} values according to Eq. (10), (+)

To establish a general rule for the behavior of the diffusion parameters D and M, simulations were performed in which the size of the domains varied (r varied from 4.5 l.s. to 36.4 l.s.) and for three values of the beam radius (R = 12 l.s., 16 l.s. and 25 l.s.). In all cases, and in particular for the smallest hexagons, good fits of the simulated recovery curves to the diffusion equations were obtained, thus enabling the mobile fraction M and the apparent diffusion coefficient D_{app} to be determined accurately. The quality of data fitting is shown in Fig. 4 for the case r = 9.09 l.s. and R = 16 l.s. The M and D_{app} values so obtained are reported in Figs. 5 A and 5 B. The main result, which will be analyzed in detail for each parameter, is that for a given value of R, M increased while D decreased with increasing r.

Mobile fraction

For the three R values tested and as shown in Fig. 5 A, the mobile fraction M was observed to increase linearly (correlation coefficient r > 0.997 in all cases) with increasing r up to a certain value r_{lim} of r (r_{lim} = 13.6 l.s. for R = 12 l.s.; r_{lim} = 16.4 l.s. for R = 16 l.s.; r_{lim} = 23.6 l.s. for R = 25 l.s.). These three linear plots can be assembled in Fig. 6 on a master straight line (r = 0.998) leading to the relationship:

$$M \cdot R = A \cdot r - B \quad (1)$$

with A = 0.634±0.004 and B = 0.709±0.043 l.s.

From this equation, it is seen that M is zero for r_0 = 1.118 l.s., a radius close to the theoretical one of 0.909 l.s. calculated for the smallest hexagon which could be used in the simulation experiments. The hexagon, 1 l.s. in side, contains only one obstacle-free site and therefore cannot show fluorescence recovery after the photobleaching step. From this, it is seen that Eq. (1) can be rewritten in the more general form:

$$M \cdot R = A \cdot (r - r_0) \quad (2)$$

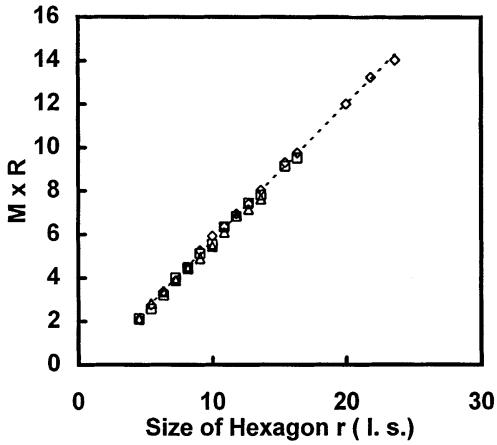

Fig. 6 Simulated FRAP experiments with closed domains. Plot of M×R values versus the hexagon size r. These values were obtained from the linear part of the plots M versus r in Fig. 5 A. R was 12 l.s. (△), 16 l.s. (□) and 25 l.s. (◇)

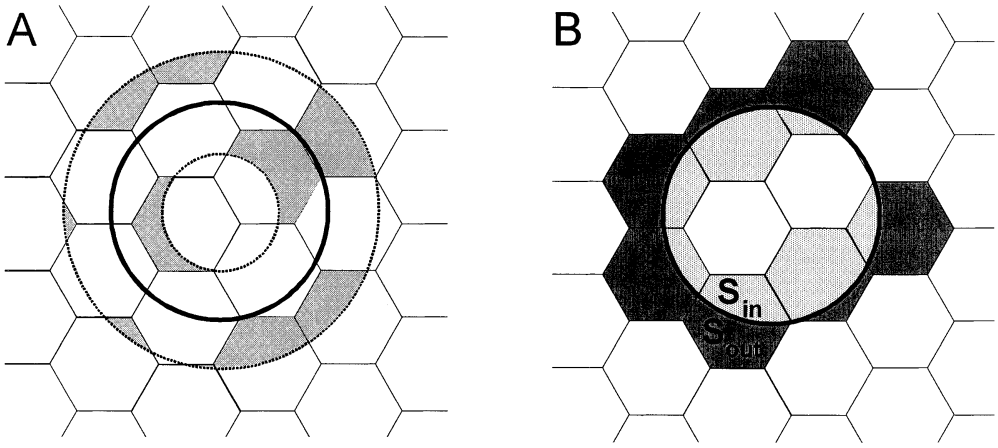

Fig. 7 A, B Simulated FRAP experiments with closed domains. In **A** and **B** the continuous circle of radius R delineates the observation area. In **A**, the dotted circles delineate the crown of inner radius (R – r) and outer radius (R + r) (see text). The tracers, which belong to those hexagons which intersect the crown (*light gray*) but do not straddle the contour of the observation area, do not participate to the recovery process. In **B**, one considers only the hexagons which straddle the contour of the observation area, i. e. those which contribute to the recovery process. The redistribution of the non-bleached tracers present in the outer surface S_{out} (*dark gray*) of the hexagons occurs over the whole surface $S_{in} + S_{out} = S$ of the hexagons. S_{in} is shown in light gray

in which r_0 designates the radius of the smallest domain which can be identified in the membrane system studied. Applying this equation to the simulation data yielded the expected size for the various hexagons tested (Standard deviation = 3.6%).

Equations (1) or (2) differ from previous analytical approximations (Yechiel and Edidin 1987; Schram et al. 1994) in which A was taken as equal to 1. The calculation developed by Schram et al. (1994) was based on the assumption that, statistically, the peripheral closed diffusion areas have half of their area intersecting the observation area and consequently 25% of all the tracers contained in the crown of inner radius (R – r) and outer radius (R + r) contribute to the recovery. In fact, this leads to an overestimation of M. Indeed, and as can be seen in Fig. 7 A the tracers which belong to the hexagons which intersect the crown (inside and outside the observation area) but do not overlap the contour of the bleaching area do not take part in the recovery. Their relative proportion is not negligible but cannot be calculated in a simple manner so no analytical formulation for the constant A could be found. However, the constant A is a geometric factor whose value can be evaluated through computational image analysis of the various surfaces to be considered (Fig. 7 B). The mobile fraction M is defined as:

$$M = N_\infty / N_0 \tag{3}$$

in which N_∞ and N_0 are the final and initial number of tracers inside the observation area, respectively. Taking the surface concentration of the tracers as being equal to 1, N_0 is given by:

$$N_0 = \sum_{\substack{\text{internal}\\ \text{domains}}} S + \sum_{\substack{\text{peripheral}\\ \text{domains}}} S_{in} \tag{4}$$

As already mentioned, only the hexagons which straddle the observation area contribute to the tracer recovery and therefore N_∞ is given by:

$$N_\infty = \sum_{\substack{\text{peripheral}\\ \text{domains}}} \frac{S_{in} \cdot S_{out}}{S} \tag{5}$$

In these equations, S is the area of one hexagon. S_{in} and S_{out} refer to the peripheral hexagons and are the areas of their surfaces which are inside and outside the observation area respectively ($S_{in} + S_{out} = S$). For each condition tested, defined by the couple r and R, 40 different positions of the observation area with respect to the hexagon network were analyzed. This yielded a value of 0.67±0.05 for the constant A, similar to the value of 0.634 deduced from the simulated FRAP experiments. In addition, the determination of M by image analysis was extended to closed cavities of various geometry. Provided the cavities displayed central symmetry, results were as above: Eq. (1) was valid up to the same values r_{lim} of r and the constant A showed little dependency on the shape of the cavities. Thus, A increased by only 25% for cavities in which the ratio of the longest to the shortest dimension was as large as 5.

For the analysis of the mobile fractions obtained by FRAP on cell membranes, Eq. (2) is to be used. The smallest domains which can be found in a membrane correspond to one molecule of lipid or of protein surrounded by its neighbors whose the size is negligible compared to that of the presumed micron-sized domains. Therefore, and for a membrane composed of strictly closed domains of size r, the changes in M with R will fit an equation of the type:

$$M = A \cdot r/R \quad \text{with} \quad M \to 0 \ \text{ for } \ 1/R \to 0 \tag{6}$$

From another point of view and on account of recent observations which suggest the existence of fluctuating barriers (Kusumi and Sako 1996, Sheets and Jacobson

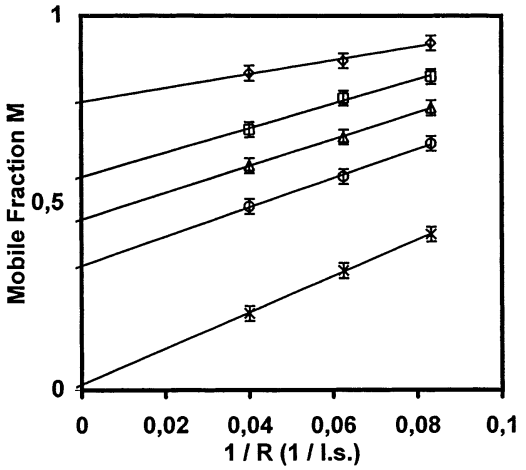

Fig. 8 Simulated FRAP experiments with slightly open domains. Plot of the mobile fraction M versus the reciprocal of the beam radius R. Hexagons of size r = 8.18 l.s. were used. Opening was as follows: 5 doors of size 2 sites (◇), 5 doors of size 1 site (□), 3 doors of size 1 site (△), 2 doors of size 1 site (○), no door (×)

1997), the membrane may be seen as being composed of domains which are not strictly closed but of the open type ("corrals" with open barriers). In this case, the mobile fraction is expected to be the sum of two terms: (i) a permanent one Mp, related to the particles which may move over long distances and which is independent of R; (ii) the other, related to those particles which remain confined in the domains during the observation time, and which depends on R. To test this hypothesis and as a first approach, open corrals were simulated with hexagons of size r = 8.18 l.s. (h = 9 l.s.) opened, on the average, as follows: 5 doors of size 2 sites (5d-2s), 5 doors of size 1 site (5d-1s), 3 doors of size 1 site (3d-1s), and 2 doors of size 1 site (2d-1s). FRAP experiments were simulated with R = 12, 16 and 25 l.s. Because long range diffusion now occurred in the total diffusion area, Io was corrected for the number of bleached tracers in the observation area with respect to the total number of tracers. In all cases, and for the simulation time of 1500 time-steps used, M was observed to increase linearly with increasing 1/R ($r > 0.995$) (Fig. 8). For $1/R \rightarrow 0$, these linear plots extrapolated at Mp values of 0.333, 0.456, 0.561 and 0.770, for the configurations 2d-1s, 3d-1s, 5d-1s and 5d-2s, respectively. For the strictly closed hexagonal domain of size 8.18 l.s., extrapolation gave an Mp value of 0.019, close to zero as expected.

The increase in Mp with increasing barrier permeability was accompanied by a progressive decrease in the slope of the straight lines. This is due to the fact that analysis now concerns only a fraction of the diffusing species, i. e., those which stay within the domains. From these results, the changes in M with R can now be accounted for by an equation of the type:

$$M = A \cdot (r_{app} - r_0)/R + Mp \quad \text{with} \quad M \rightarrow Mp \quad \text{for} \quad 1/R \rightarrow 0 \qquad (7)$$

which yields an apparent value r_{app} for the radius of the domains. This value is slightly under-estimated as compared to the real value r introduced in the simulations. For example, the slope of the line extrapolating at Mp = 0.333 in Fig. 8, yields an r_{app} value of 7.26 l.s., which differs by only 11% from the real value r = 8.18 l.s. used in the simulations.

Diffusion coefficient

The diffusion coefficients plotted in Fig. 5 B were calculated with the assumption that the diffusion of the tracers occurred all over the observation area S_{obs} which is obviously not correct and, in fact, leads to an apparent diffusion coefficient D_{app}. However, if the real diffusion area is known, the real diffusion coefficient D_0 inside the closed cavities can be obtained from the data. Obviously, D_0 should be independent of r and R. Since the diffusion of all the tracers is reduced to the domain to which they belong, the real diffusion area S_{diff} is half that of a closed cavity. Indeed, the domains which overlap the observation area are centered statistically on its perimeter, which means that 50% of the surface of these domains are observed inside the observation area. The characteristic time of diffusion τ_D, which characterizes the dynamics of the recovery process is given as:

$$\tau_D = \langle l^2 \rangle / 4\, D \qquad (8)$$

in which $\langle l^2 \rangle$ is the mean square displacement. Therefore, one can write:

$$\tau_D \approx S_{obs}/4\, D_{app} \approx S_{diff}/4\, D_0 \qquad (9)$$

In our case, $S_{obs} = \pi R^2$ and $S_{diff} = 1/2\, \pi r^2$ which leads to:

$$D_0 \approx 1/2\, D_{app} (r/R)^2 \qquad (10)$$

The D_0 values calculated from the data in Fig. 5 B with the help of Eq. (10) are shown in the same figure. They were found to be independent of r and R and equal to 0.362±0.039 u. This value was close to that of 0.326± 0.007 u, previously obtained for an obstacle-free lattice and using the same numerical simulations (Schram et al. 1994), thus demonstrating the validity of Eq. (10).

For membranes strictly composed of closed domains, the various fluorescence recoveries recorded for lipids and proteins for various R values are expected to be accounted for by one diffusion coefficient D_{app} and these D_{app} values are expected to show a quadratic dependence on R and to yield, with the help of Eq. (10), the real diffusion coefficient D_0 inside the domains. For membranes composed of slightly open domains, the fluorescence recoveries are expected to be fitted with two diffusion coefficients: (i) one, independent of R and corresponding to the particles which diffuse over long distances; (ii) another one, showing a quadratic dependence on R and corresponding to the particles inside the domains. Accordingly, the simulated recoveries obtained for the open domains of various size examined were well fitted with two diffusion coefficients, one exhibiting the expected independence of R and the other the quadratic dependence on R (data not shown).

Monolayers of silica beads supporting a "hairy" phospholipid bilayer

The formation of SSB monolayers was checked first by direct observation in the fluorescence microscope. Several regions exhibiting hexagonal packing of the spheres could be found on the slides and FRAP experiments were carried out on these well organized regions only.

Monolayers of silica beads coated with a phospholipid bilayer constitute a good experimental model of a membrane organized in strictly closed lipid domains provided the bilayers on adjacent beads are independent of each other. In other words, this means the lateral diffusion of lipids is restricted to the surface of each bead and no long range diffusion from bead to bead occurs.

Surprisingly, without addition of PEG5000-eggPE to the lipids, long range diffusion was observed. With a beam radius of 4.2 μm, much larger than the radius of silica beads (0.83 μm), a diffusion coefficient of $0.6\pm0.1\ 10^{-8}$ cm^2 s^{-1} and a mobile fraction of 100% were measured, indicating that extensive fusion had occurred between adjacent spherical bilayers. This observation is consistent with that of Helm et al. (1989) who showed that fusion occurs spontaneously between amphiphilic bilayers once their surfaces come within one nanometer. A diffusion coefficient of $1.2\pm0.2\ 10^{-8}$ cm^2 s^{-1} and a mobile fraction of 100% were measured on planar supported bilayers with the same lipid composition. As already discussed in the case of microvilli of the surface of plasma membranes (Aizenbud et al. 1982), the factor of ~2 between the two D values may be explained by the fact that for SSB, analysis of the fluorescence recovery curves is carried out by considering not the real area $2\pi r^2$ of the hemi-spherical bilayers in contact with the beads but their planar projection πr^2.

To prevent fusion between the spherical bilayers, a spacer was used, namely PEG5000-eggPE and SSB were prepared with increasing concentrations of this lipid (1 mol% increments). To check whether the absence of fusion was satisfied, manual photobleaching experiments were carried out using the field diaphragm of the microscope. In the absence of long range diffusion, (i) the area in which bleached probes can be found should not extend beyond the observation area, even for long illumination times, and (ii) fluorescence recovery should not be detected at the center of the bleached area, at least within 15 min after a short bleaching period. To avoid artifacts, these tests were performed on well organized regions of great size (at least 5 times the size of the observation area). In this way long range diffusion indicative of membrane fusion was observed up to 4 mol% PEG5000-eggPE, and ceased at a concentration of 5 mol%. In this condition and with a beam radius of 4.2 μm, no significant fluorescence recovery was observed. In contrast, with a small observation radius of 1.05 μm, a significant fluorescence recovery was measured, indicating that lateral diffusion of lipids still occurred around the beads. To check whether PEG5000-eggPE did not strongly alter the lateral diffusion of the host lipid, FRAP experiments were carried out on planar supported bilayers with the same lipid composition (5 mol% PEG5000-eggPE plus 2 mol% NBD-eggPE in eggPC). A diffusion coefficient of $0.5\pm0.1\ 10^{-8}$ cm^2 s^{-1} and a mobile fraction of 100% were measured, indicating that at the concentration of 5 mol%, PEG5000-eggPE only slightly reduced the lateral diffusion rate of the host lipids. From these experiments, it can be concluded that in the presence of 5 mol% PEG5000-eggPE, the lateral diffusion of lipids was restricted to the spherical bilayers around the beads, as expected. Several preparations were needed to perform the whole study and the above mentioned control FRAP experiment were repeated for each of them.

Taking into account the radius r = 0.83 μm of the silica beads and the sensitivity of our FRAP apparatus (for mobile fractions less than 20%, the signal to noise ratio became too low for a correct analysis of the recovery curves), three values of the observation radius were used in the interesting range R > r, i.e. R = 1.05 μm, 1.45 μm and 1.95 μm. For each value of R, the 30 fluorescence recoveries recorded showed a noise comparable to that encountered with any FRAP experiment and accounted for bidimensional diffusion. However, when the bleaching spot was moved, great dispersion in the asymptotic value of M was observed from one recovery to the other (±60%). This was due to changes in the relative position of the bleaching area and the SSB network. For that reason and for each R value tested, the 30 recovery curves were averaged. The resulting curves are shown in Fig. 9. Because of the sphericity of the lipid bilayers, it was difficult to analyze the FRAP data using the diffusion equations which have been derived for planar systems. M was determined graphically as the asymptotic value of the averaged recovery curves (Fig. 9) and the apparent diffusion coefficient D_{app} was estimated from the fluorescence recovery half time $t_{1/2}$ measured on these curves and using the relation $D = 0.22\ R^2/t_{1/2}$ (Axelrod et al. 1976). Results are reported in Fig. 10 and Table 1.

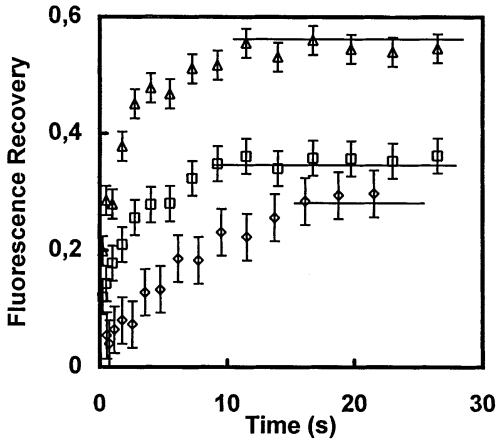

Fig. 9 Experimental FRAP experiments. Fluorescence recovery curves obtained on monolayers of spherical supported "hairy" phospholipid bilayers (SSB) for three different observation radius R: 1.05 μm (△), 1.45 μm (□) and 1.95 μm (◇). Each curve is the average of 30 measurements

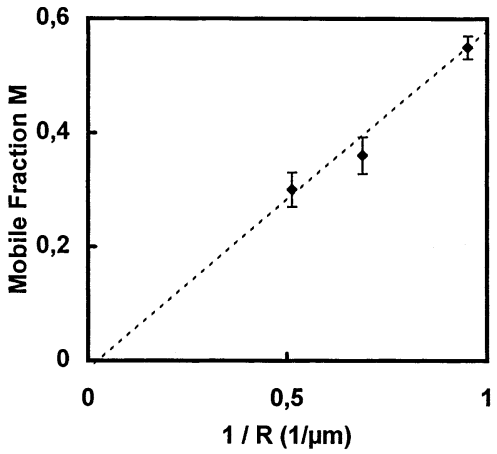

Fig. 10 Experimental FRAP experiments. Plot of the mobile fraction M versus the reciprocal of the beam radius R measured by FRAP experiments on monolayers of spherical supported "hairy" phospholipid bilayers (SSB) labeled with NBD-eggPE

Table 1 Mobile fractions and diffusion coefficients obtained by FRAP experiments on monolayers of silica beads supporting an egg-PC bilayer containing 5 mol% PEG5000-eggPE, for various values of the beam radius R. Also shown are the mobile fractions determined by image analysis (see text)

R (μm)	$M_{experimental}$	$M_{calculated}$	D_{app} (10^{-8} cm^2 s^{-1})	D_0 (10^{-8} cm^2 s^{-1})
1.05	0.55±0.02	0.52±0.06	0.32±0.06	0.23±0.07
1.45	0.36±0.03	0.42±0.04	0.46±0.07	0.21±0.05
1.95	0.30±0.03	0.32±0.02	–	–

As can be seen in Fig. 10, the mobile fraction M decreased with increasing R. It should be stressed that FRAP experiments were carried out with a ×63/1.3 oil-immersion objective whose depth of focus of ≈1.5 μm (Dupou et al. 1988) was comparable to the diameter of the spherical bilayers. In these conditions, the measured fluorescence intensities accounted for all the fluorescent probes present in the spherical bilayers which were included in the observation area. The data in Fig. 10 falls on a straight line with the equation $M = (0.58\pm0.08)/R - (0.01\pm0.07)$ ($r = 0.984$). As expected for such a system, this corresponds to an equation of the type of Eq. (5), with a mobile fraction extrapolating at 0 for $1/R \rightarrow 0$, indicating strictly closed diffusion areas. From the slope, a radius of 0.92±0.09 μm was calculated for the spherical bilayers which compared well with the radius of 0.83 μm given for the supporting silica beads. As a control experiment, the mobile fractions were calculated by image analysis as described above. Images of lattices of disks with the same arrangement as in SSB monolayers were generated and the theoretical values of M were determined for the three r/R ratios used. In each case, 10 different positions of the observation area with respect to the lattice were considered. The images observed corresponded to planar projections of spherical surfaces. Using simple geometric calculations, the area of these planar surfaces was converted into the area of the corresponding real spherical surfaces. As can be seen in Table 1, the M values calculated in this way are in good agreement with the experimental ones.

With respect to the diffusion coefficient, and if one refers to the numerical simulations, D_{app} should increase with increasing R. This was indeed the case for R = 1.05 μm and 1.45 μm (Table 1). Unfortunately, D_{app} could not be determined accurately for R = 1.95 μm because the signal to noise ratio was too low in this case.

To evaluate the diffusion coefficient D_0 from D_{app}, the average fraction F_{in} of the area of the peripheral SSB which is inside the observation radius was determined. F_{in} values of 0.29±0.03 and 0.35±0.03 were found for R = 1.05 μm and 1.45 μm, respectively. The real diffusion area S_{diff} is $S_{diff} = F_{in}\, 4\pi r^2$ which leads to the following expression for D_0:

$$D_0 \approx 4\, F_{in} \cdot D_{app}\, (r/R)^2 \qquad (11)$$

Consistently, and within the limits of the accuracy of our experiments, the two calculated values of D_0 were found to be identical and equal to $0.2 \cdot 10^{-8}$ cm^2 s^{-1} (Table 1). Taking into account the differences in nature and curvature between the supports and the way the diffusion coefficients were calculated, this value of D_0 compares well with the diffusion coefficient of $0.5 \cdot 10^{-8}$ cm^2 s^{-1} found for planar supported bilayers of the same composition.

Discussion

The above numerical simulations of FRAP experiments at variable observation radius R on compartmentalized membranes allowed us to establish the relationships which exist between (i) the mobile fractions M and the size r of membrane domains, and (ii) the apparent diffusion coefficient D_{app} and the real diffusion coefficient D_0 inside the domains. According to these simulations, the existence of domains in membranes can be inferred from FRAP measurements at variable beam radii by plotting M versus 1/R. A linear relationship between M and 1/R, at low values of 1/R, together with a quadratic increase of D_{app} with R are the signature of the presence of such domains. If the linear part of the plot extrapolates at M = 0 for $1/R \rightarrow 0$, the domains can be considered as being closed, at least over the time scale of the FRAP experiments. If extrapolation indicates a permanent mobile fraction Mp, then the domains are not strictly closed. In all cases, the average size r of the domains can be determined with the help of Eq. (6) or (7) from the slope of the linear part of the M versus 1/R plots. For closed domains, the diffusion coefficient D_0 inside the domains can be deduced from the changes of D_{app} with R using Eq. (10). The validity of this approach was tested through the analysis of the experimental FRAP data obtained with a model of a compartmentalized membrane.

It should be stressed that despite its complex geometry, the system consisting of monolayers of silica beads supporting a "hairy" phospholipid bilayer, proved to be a good model of a membrane partitioned into closed lipid domains and quite useful for testing our theoretical predictions. On this membrane model system, our approach indicated the presence of strictly closed domains whose size was as expected. It is also worth noting that an extensive fusion was observed between adjacent spherical bilayers and that a relatively high PEG5000-eggPE mole fraction of 5% was necessary to hinder the fusion process. This value is higher than that which corresponds to the limit of overlapping of the PEG polymer chains and which can be evaluated at ≈2% from literature data (Kuhl et al. 1994, Janzen et al. 1996). This means that in our case, the PEG chains were in the strongly-overlapping "brush" regime in which the chains are elongated (de Gennes 1988). The fact that both this chain conformation and a relatively high PEG5000-eggPE concentration were required to achieve an efficient steric barrier between adjacent lipid bilayers corroborates the conclusion of Kuhl et al. (1994) stating that a good protection of the lipid surface in liposomes requires not only a minimum thickness of the polymer layer (after the transition to the brush regime the thickness of the polymer layer increases abruptly beyond the Flory radius of a chain) but also a dense polymer layer.

Experimental FRAP data at variable beam radii on living cells is scarce but fortunately concerns both lipids and proteins, which makes a comparison between the behavior of the two classes of molecules possible. The up-to-date available mobile fraction data obtained for lipids and proteins in the plasma membrane of human skin fibroblasts (Yechiel and Edidin 1987) and mouse hepatoma cells (Edidin and Stroynowski 1991) are plotted versus 1/R in Figs. 11 A and 11 B respectively. For both lipids and proteins M is seen to increase linearly ($0.827 < r < 0.98$) with 1/R in the region of low 1/R values and to extrapolate to a value of $Mp \sim 0.2$ for $1/R \rightarrow 0$. Consistently, analysis of these plots with Eq. (7) suggests the presence of micron-sized domains (Table 2), which are not strictly closed but of the open type. In agreement with the existence of domains, D_{app} was observed to increase with R. Unfortunately, the real diffusion coefficient D_0 cannot be obtained

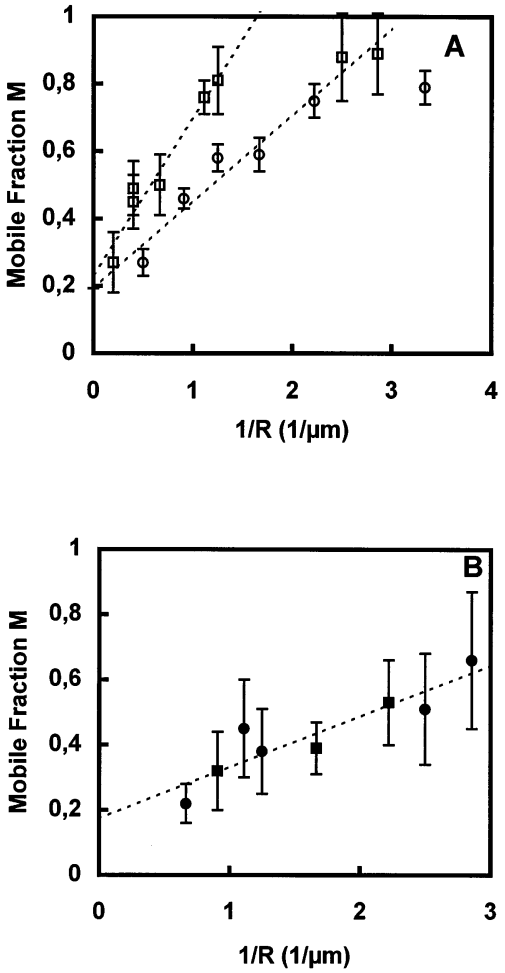

Fig. 11A, B Experimental FRAP experiments. Plot of the mobile fraction M versus the reciprocal of the beam radius R measured for different probes in various plasma membranes. **A** lipid analog NBD-PC (○) in the plasma membrane of human skin fibroblasts (Yechiel and Edidin 1987); lipid analog NBD-PC (□) in the plasma membrane of mouse hepatoma cells (Edidin and Stroynowski 1991). **B** Fl-Fab labeled proteins (●) in the plasma membrane of human skin fibroblasts (Yechiel and Edidin 1987) and Fl-Fab labeled H-2Db protein (■) in the plasma membrane of mouse hepatoma cells (Edidin and Stroynowski 1991). The straight lines which fit the experimental data at low 1/R values were those used to calculate the size of the domains (see text and Table 2)

Table 2 Radius r of the closed domains identified through the analysis with Eq. (7) of FRAP data obtained at variable beam radii, for proteins and lipids in the plasma membrane of various cellular systems. Also given are the correlation coefficient (r) qualifying the plots M vs 1/R in Figs. 11 A and 11 B, and the permanent mobile fraction Mp obtained for $1/R \rightarrow 0$ (see text and Figs. 11 A and 11 B)

Cells	Lipids			Proteins		
	r (μm)	(r)	Mp	r (μm)	(r)	Mp
Human skin fibroblast (Yechiel and Edidin 1987)	0.74±0.20	0.95	0.23±0.05	0.25±0.10	0.83	0.18±0.05
Mouse hepatoma (Edidin and Stroynowski 1991)	0.41±0.20	0.92	0.19±0.05	0.25±0.10	0.92	0.16±0.05

from this data. Indeed, and because of the presence of a permanent mobile fraction Mp, calculation of D_0 would have required an analysis of the fluorescence recovery curves with two diffusion coefficients. These curves were not published.

In the plasma membranes of human skin fibroblasts and mouse hepatoma, domains probed by lipids exhibit an apparent radius of around 0.7 and 0.4 μm respectively (Fig. 11 A, and Table 2).

With respect to proteins, the FRAP data obtained for human skin fibroblasts and mouse hepatoma can be assembled on the same line (Fig. 11 B) and indicates domains of about 0.25 μm in radius. This is in agreement with recent results obtained by analyzing the lateral motion of transmembrane proteins (principally membrane receptors) at the surface of various cell types using a Single Particle Tracking (SPT) technique (Saxton and Jacobson 1997) and which accounts for domains with radii in the 0.1–0.5 μm range (Sheets et al. 1995). More precisely and to make the comparison with fibroblastic cells, domains of 0.26 μm and 0.36 μm in radius have been identified in the plasma membrane of rat kidney fibroblasts by tracking the movements of transferrin and α_2-macroglobulin receptors respectively (Sako and Kusumi 1994). Domains of 0.16 μm in radius were observed by tracking the GPI-anchored protein Thy-1 at the surface of C3H fibroblasts (Sheets and Jacobson 1997).

With respect to the structure of membrane domains, one current opinion is to consider that confinement of proteins in domains is principally due to interactions of the cytosolic part of these molecules with membrane skeleton and/or cytoskeleton elements (Kusumi and Sako 1996). Owing to thermal fluctuations which modulate the distance between the membrane and the skeleton meshwork, proteins can move from one domain to the next or undergo random or directed long-range motions (Kusumi and Sako 1996). In this model, the barriers to protein diffusion are located outside the membrane, not within the membrane. In the absence of intra-membrane barriers, membrane proteins may be assumed to behave like randomly distributed obstacles to the lateral motion of lipids. A slowing down of the lateral diffusion rate of lipids is expected, not a restriction of their long-range motions, as was observed with reconstituted proteoliposomes (Cherry 1979, Schram et al. 1994). In fact, the existence of lipid domains in membranes whose size is comparable to that of protein domains implies the presence of intra-membrane barriers. More than likely, membrane proteins are the origin of these barriers (Edidin 1993, Tocanne et al. 1994 a) and in addition to interactions with the membrane skeleton, attractive interprotein interactions may contribute to the stabilization of fences (Abney and Scalettar 1995). Today membranes cannot be seen as static structures (Edidin 1993). Instead, a dynamic model of membranes consisting of a network of fluctuating and size-selective barriers may be proposed. The concept of fluctuating barriers is sustained by theoretical simulations of protein distribution in membranes (Abney and Scalettar 1995), and experimentally by SPT experiments which show residence times of proteins in given domains in the range 3–30 s (Sheets et al. 1995; Saxton and Jacobson 1997). Note that 3–30 s is the typical time scale of FRAP experiments which consistently indicate an absence of long-range diffusion for the proteins. Because of thermal fluctuations, the barrier network is likely to depend on local fluctuations in the distribution and surface density of lipid and protein molecules (Abney and Scalettar 1995). On the average, and taking into account the relative size of the diffusing species, the barriers are expected to be more permeable to lipids as compared to proteins. In agreement with our simulation experiments, fluctuating barriers may explain the existence of a permanent mobile fraction Mp which accounts for the possibility that a fraction of protein and lipid molecules may undergo long-range lateral diffusion. Size selective barriers may explain why domains probed by lipids and proteins differ in size within the same membrane. Accordingly, it is worth stressing that in the plasma membrane of fibroblasts and mouse hepatoma, domains were of greater radius when probed by lipids (0.4–0.7 μm) than when probed by proteins (0.25 μm). It should be observed that if these membranes were composed of strictly closed and juxtaposed domains then, proteins and lipids which are free to diffuse laterally within these domains would report the same size. Finally, and at its present stage of development, the simulation data suggests that the permanent mobile fraction of 20% observed in cells would account for only a very low extent of opening of the barriers. Thus, an Mp value of 33% was found for hexagons of size r = 8.18 l.s. with (on the average) 2 doors of 1 l.s. which represent only ≈5% of the hexagon perimeter.

Conclusion

The FRAP technique is of considerable interest for investigating the lateral organization of membranes because it can be used to study the cell surface mobility of both lipids and proteins. We have demonstrated here that performing a run of experiments at variable beam radii gives information on both the dynamics and structure of membranes. It provides evidence of compartmentalization if it exists, and allows for the determination of the size of the domains and the diffusion coefficient inside the domains. The next step is to consider the dynamics of the system and to introduce the concept of barriers which are fluctuating and selective in size with respect to lipid and protein molecules. This work is in progress in our laboratory.

References

Abney JR, Scalettar BA (1995) Fluctuations and membrane heterogeneity. Biophys Chem 57: 27–36

Aizenbud BM, Gershon ND (1982) Diffusion of molecules on biological membranes of nonplanar form. Biophys J 38: 287–293

Axelrod D, Koppel DE, Schlessinger J, Elson E, Webb WW (1976) Mobility measurement by analysis of fluorescence photobleaching recovery kinetics. Biophys J 16: 1055–1069

Bayerl TM, Bloom M (1990) Physical properties of single phospholipid bilayers adsorbed to micro glass beads. Biophys J 58: 357–362

Cherry RJ (1979) Rotational and lateral diffusion of membrane proteins. Biochim Biophys Acta 559: 289–327

De Bony J, Lopez A, Gilleron M, Welby M, Lanéelle G, Rousseau B, Beaucourt JP, Tocanne JF (1989) Transverse and lateral distribution of phospholipids and glycolipids in the membrane of the bacterium *Micrococcus luteus*. Biochemistry 28: 3728–3737

De Gennes PG (1988) Model polymers at interfaces. In: Bongrand P (ed) Physical basis of cell-cell adhesion. CRC Press, Boca Raton, Florida, pp 91–123

Dupou L, Lopez A, Tocanne JF (1988) Comparative study of the lateral motion of extrinsic probes and anthracene-labelled constitutive phospholipids in the plasma membrane of Chinese hamster ovary cells. Eur J Biochem 171: 669–674

Edidin M, Stroynowsky I (1991) Differences between the lateral organization of conventional and inositol phospholipid-anchored membrane proteins. A further definition of micrometer scale membrane domains. J Cell Biol 112: 1143–1150

Edidin M (1993) Patches and fences: probing for plasma membrane domains. J Cell Sci 17: 165–169

Feder TJ, Brust-Mascher I, Slattery JP, Baird B, Webb WW (1996) Constrained diffusion or immobile fraction on cell surface: a new interpretation. Biophys J 70: 2767–2773

Helm CA, Israelachvili JN, McGuiggan PM (1989) Molecular mechanisms and forces involved in the adhesion and fusion of amphiphilic bilayers. Science 246: 919–922

Jacobson KE, Sheets D, Simson R (1995) Revisiting the fluid mosaic model of membranes. Science 268: 1441–1442

Janzen J, Song X, Brooks DE (1996) Interfacial thickness of liposomes containing poly(ethylene glycol)-cholsterol from electrophoresis. Biophys J 70: 313–320

Kalb E, Frey S, Tamm LK (1992) Formation of supported planar bilayers by fusion of vesicles to supported phospholipid monolayers. Biochim Biophys Acta 1103: 307–316

Kuhl TL, Leckband DE, Lasic DD, Israelachvili JN (1994) Modulation of interaction forces between bilayers exposing short-chained ethylene oxide headgroups. Biophys J 66: 1479–1488

Kusumi A, Sako Y (1996) Cell surface organization by the membrane skeleton. Curr Opin Cell Biol 8: 566–574

Lopez A, Dupou L, Altibelli A, Trotard J, Tocanne JF (1988) Fluorescence recovery after photobleaching (FRAP) experiments under conditions of uniform disk illumination. Biophys J 53: 963–970

Mouritsen OG, Jorgensen K (1997) Small-scale lipid-membrane structure: simulation vs experiment. Curr Opin Struct Biol (in press)

Sako Y, Kusumi A (1994) Compartmentalized structure of the plasma membrane receptor movements as revealed by a nanometer-level motion analysis. J Cell Biol 125:1251–1264

Sako Y, Kusumi A (1995) Barriers for lateral diffusion of transferrin receptor in the plasma membrane as characterized by receptor dragging by laser tweezers: fence versus tether. J Cell Biol 129: 1559–1574

Saxton MJ, Jacobson K (1997) Single-particle tracking: application to membrane dynamics. Annu Rev Biophys Biomol Struct 26: 371–397

Schram V, Tocanne JF, Lopez A (1994) Influence of obstacles on lipid lateral diffusion: computer simulation of FRAP experiments and application to proteoliposomes and biomembranes. Eur Biophys J 23: 337–348

Sheets ED, Simson R, Jacobson K (1995) New insights into membrane dynamics from the analysis of cell surface interactions by physical methods. Curr Opin Cell Biol 7: 707–714

Sheets ED, Jacobson K (1997) Transient confinement of GPI-anchored proteins by glycolipid membrane domains. Biophys J 72: A67

Simson R, Sheets ED, Jacobson K (1995) Detection of temporary lateral confinement of membrane proteins using single particle tracking analysis. Biophys J 69: 989–993

Sweet WD, Schroeder F (1988) Lipid domains and enzyme activity. In: Aloia RC, Curtain CC, Gordon LM (eds) Lipid domains and the relationship to membrane function. Liss, pp 17–42

Tocanne JF (1992) Detection of lipid domains in biological membranes. Comments Mol Cell Biophys 8: 53–72

Tocanne JF, Cézanne L, Lopez A, Piknova B, Schram V, Tournier JF, Welby M (1994a) Lipid domains and lipid/protein interactions in biological membranes. Chem Phys Lipids 73: 139–158

Tocanne JF, Dupou-Cézanne L, Lopez A (1994b) Lateral diffusion of lipids in model and natural membranes. Prog Lipid Res 33: 203–237

Vaz WLC, Derzko ZI, Jacobson KA (1982) Photobleaching measurements of the lateral diffusion of lipids and proteins in artificial phospholipid bilayer membranes. In: Poste G, Nicholson GL (eds) Cell surface reviews, vol 8. Elsevier Biomedical Press, Amsterdam, pp 83–137

Welby M, Poquet Y, Tocanne JF (1996) The spatial distribution of phospholipids in the membrane of the bacterium Micrococcus luteus varies during the cell cycle. FEBS Letters 384: 107–111

Welti R, Glaser M (1994) Lipid domains in model and biological membranes. Chem Phys Lipids 73: 121–137

Yechiel E, Edidin M (1987) Micrometer-scale domains in fibroblast plasma membranes. J Cell Biol 105: 755–760